

---

Erik Jonsson School of Engineering and Computer Science

---

2013-09-12

*Chemical and Electrical Characterization of the  
HfO<sub>2</sub>/InAlAs Interface*

UTD AUTHOR(S): Barry Brennan, Rohit V. Galatage, Jiyoung Kim.  
Christopher L. Hinkle and Robert M. Wallace

©2013 AIP Publishing LLC.

## Chemical and electrical characterization of the HfO<sub>2</sub>/InAlAs interface

B. Brennan, R. V. Galatage, K. Thomas, E. Pelucchi, P. K. Hurley, J. Kim, C. L. Hinkle, E. M. Vogel, and R. M. Wallace

Citation: [Journal of Applied Physics](#) **114**, 104103 (2013); doi: 10.1063/1.4821021

View online: <http://dx.doi.org/10.1063/1.4821021>

View Table of Contents: <http://scitation.aip.org/content/aip/journal/jap/114/10?ver=pdfcov>

Published by the [AIP Publishing](#)

---

### Articles you may be interested in

Characterization of atomic layer deposition HfO<sub>2</sub>, Al<sub>2</sub>O<sub>3</sub>, and plasma-enhanced chemical vapor deposition Si<sub>3</sub>N<sub>4</sub> as metal–insulator–metal capacitor dielectric for GaAs HBT technology

J. Vac. Sci. Technol. A **31**, 01A134 (2013); 10.1116/1.4769207

Effective passivation of In<sub>0.2</sub>Ga<sub>0.8</sub>As by HfO<sub>2</sub> surpassing Al<sub>2</sub>O<sub>3</sub> via in-situ atomic layer deposition

Appl. Phys. Lett. **101**, 172104 (2012); 10.1063/1.4762833

Electrical analysis of three-stage passivated In<sub>0.53</sub>Ga<sub>0.47</sub>As capacitors with varying HfO<sub>2</sub> thicknesses and incorporating an Al<sub>2</sub>O<sub>3</sub> interface control layer

J. Vac. Sci. Technol. B **29**, 01A807 (2011); 10.1116/1.3532826

Structural and electrical analysis of the atomic layer deposition of HfO<sub>2</sub> / n -In<sub>0.53</sub>Ga<sub>0.47</sub>As capacitors with and without an Al<sub>2</sub>O<sub>3</sub> interface control layer

Appl. Phys. Lett. **97**, 052904 (2010); 10.1063/1.3473773

Atomic-layer-deposited HfO<sub>2</sub> on In<sub>0.53</sub>Ga<sub>0.47</sub>As : Passivation and energy-band parameters

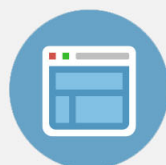
Appl. Phys. Lett. **92**, 072901 (2008); 10.1063/1.2883967

---



## Re-register for Table of Content Alerts

Create a profile.



Sign up today!



# Chemical and electrical characterization of the $\text{HfO}_2/\text{InAlAs}$ interface

B. Brennan,<sup>1</sup> R. V. Galatage,<sup>2</sup> K. Thomas,<sup>3</sup> E. Pelucchi,<sup>3</sup> P. K. Hurley,<sup>3</sup> J. Kim,<sup>1</sup> C. L. Hinkle,<sup>1</sup> E. M. Vogel,<sup>4</sup> and R. M. Wallace<sup>1,2,a)</sup>

<sup>1</sup>Department of Materials Science and Engineering, University of Texas at Dallas, Richardson, Texas 75080, USA

<sup>2</sup>Department of Electrical Engineering, University of Texas at Dallas, Richardson, Texas 75080, USA

<sup>3</sup>Tyndall National Institute, University College Cork, Lee Maltings, Prospect Row, Cork, Ireland

<sup>4</sup>School of Materials Science and Engineering, Georgia Institute of Technology, Atlanta, Georgia 30332, USA

(Received 19 June 2013; accepted 26 August 2013; published online 12 September 2013)

InAlAs has the potential to be used as a barrier layer in buried channel quantum well field effect transistor devices due to favorable lattice-matching and carrier confinement properties with InGaAs. Field effect device structures of this nature may also require a high- $k$  oxide deposited on the InAlAs surface to reduce leakage current. This study investigates the impact of surface preparations and atomic layer deposition of  $\text{HfO}_2$  on these surfaces using x-ray photoelectron spectroscopy to analyse the chemical interactions taking place, as well as the electrical performance of associated capacitor devices. A large concentration of As related surface features is observed at the InAlAs surface, and is attributed to a large  $D_{it}$  response in electrical measurements.

© 2013 AIP Publishing LLC. [<http://dx.doi.org/10.1063/1.4821021>]

## INTRODUCTION

One of the major issues in realizing a high quality III–V based field effect transistor (FET) is the poor interface quality between the III–V material of choice and high- $k$  oxides,<sup>1</sup> which generally leads to the formation of significant density of interface defect states ( $D_{it}$ ).<sup>2</sup> In surface channel metal oxide semiconductor (MOS) FET devices, As decapping, wet chemical processing using, for example, HF, HCl,  $\text{NH}_4\text{OH}$ ,<sup>3–5</sup> atomic hydrogen treatments,<sup>6,7</sup> as well as sulphur<sup>8,9</sup> and nitrogen passivations<sup>10,11</sup> have all been employed in order to remove native oxides and diminish the interaction between any deposited oxide and the semiconductor. However, while these processes have all shown improvements in device performance, the  $D_{it}$  levels are still too high to make the incorporation of a III–V channel a viable alternative to Si in the short term.

One proposed method to overcome this has been to move the III–V channel away from the oxide interface by incorporating a lattice matched buffer layer between the channel and the high- $k$  oxide.<sup>12–14</sup> InGaAs is widely studied as the channel material in these devices due to its low effective electron mass and high electron mobility.  $\text{In}_{0.52}\text{Al}_{0.48}\text{As}$ , which is lattice matched to  $\text{In}_{0.53}\text{Ga}_{0.47}\text{As}$ , has a higher conduction band offset with an InGaAs channel compared to using an InP barrier layer, and so offers the potential of improved confinement of electrons in the channel. Also, through *in-situ* epitaxial growth, a high quality interface between InGaAs and InAlAs can be obtained.<sup>15,16</sup> However, the interface between the barrier layer and high- $k$  oxide still plays an active role in device operation, having an impact on sub threshold swing<sup>9</sup> and the threshold voltage.<sup>17</sup> As such it is still necessary to characterize and investigate the surface and interface reactions that take place during surface

preparations and after subsequent oxide depositions on this surface.

In this study, the native oxides and surface states present on the initial  $\text{In}_{0.52}\text{Al}_{0.48}\text{As}$  surface, after wet chemical treatment and after deposition of a Si interfacial passivation layer (IPL) on the native oxide surface is examined using X-ray photoelectron spectroscopy (XPS). The impact of depositing  $\text{HfO}_2$  by atomic layer deposition (ALD) on these surfaces is also considered, and changes in the interfacial chemistry with XPS are monitored. Capacitance-Voltage (C–V) measurements are also performed on metal-insulator-semiconductor (MIS) capacitors incorporating  $\text{HfO}_2$  deposited on the native oxide, on the sulfur treated surface and on the Si IPL layer.

## EXPERIMENTAL

For this study, a 300 nm  $n$ -type  $\text{In}_{0.53}\text{Al}_{0.47}\text{As}$  layer (Si doped  $\sim 1 \times 10^{18} \text{ cm}^{-3}$ ) was epitaxially grown on a single crystal  $n$ -type InP substrate (S doped  $\sim 1 \times 10^{18} \text{ cm}^{-3}$ ) by metal organic vapor phase epitaxy, in a system where particular care is taken to ensure reactor purity and epitaxial step organization.<sup>18</sup> The growth pressure was 80 millibars, the V/III ratio was 220, and the wafer surface temperature was 650 °C as measured by emissivity-corrected pyrometry.  $\text{HfO}_2$  layers were deposited using tetrakis dimethylamido hafnium (TDMA-Hf) and  $\text{H}_2\text{O}$  precursors in a Picosun<sup>©</sup> ALD reactor at 250 °C, with a pulse/purge time of 0.1 s TDMA-Hf—20 s  $\text{N}_2$ —0.1 s  $\text{H}_2\text{O}$ —20 s  $\text{N}_2$  and ultra-high purity  $\text{N}_2$  as both carrier and purging gas (200 sccm). The base pressure in the ALD reactor is  $\sim 9$  millibars. The increase in pressure during  $\text{H}_2\text{O}$  and TDMA-Hf pulses was measured to be 5 millibars and 0.7 millibar, respectively.

Prior to  $\text{HfO}_2$  deposition, a series of five different surface and chemical treatments were carried out on the  $\text{In}_{0.52}\text{Al}_{0.48}\text{As}$  surface to determine the impact these would have on the native oxide present on the surface. In all cases,

<sup>a)</sup>Author to whom correspondence should be addressed. Electronic mail: [rmwallace@utdallas.edu](mailto:rmwallace@utdallas.edu)

sample degreasing was first carried out, consisting of a sequential treatment for 1 min each in acetone, methanol, and isopropanol. Ammonium hydroxide (29%  $\text{NH}_4\text{OH}$  for 3 min), ammonium sulfide (10%  $(\text{NH}_4)_2\text{S}$  for 20 min), and hydrochloric acid (18.5%  $\text{HCl}$  for 10 min) wet chemical treatments were employed, as well as the deposition of a thin ( $\sim 1$  nm) amorphous silicon IPL by plasma enhanced chemical vapor deposition (PECVD) on a sample that was initially etched in 1%  $\text{HF}$  for 2 min. The Si PECVD process employed a mixture of diluted  $\text{SiH}_4$  and He (100 sccm of 2%  $\text{SiH}_4/\text{He}$ , 400 sccm of He, 50 W, 200 °C). No sample annealing was carried out prior to PECVD and as such interaction between Si and native oxide species residual on the surface is expected. A control sample that only underwent sample degreasing was also examined, and all samples were loaded to UHV within 7 min of surface treatment. For all samples, the changes in the individual As, In, and Al oxide states were compared by XPS.

For the five differently prepared InAlAs samples undergoing XPS analysis, 15 cycles of TDMA-Hf and  $\text{H}_2\text{O}$  were deposited *in-situ* on the treated substrate (giving an approximate  $\text{HfO}_2$  thickness of 1.2 nm, with a growth rate of 0.08 nm/cycle) to prevent interfacial re-oxidation and surface contamination. Samples were transferred under UHV from the ALD reactor to a dedicated XPS analysis chamber through a transfer tube maintained at  $<1 \times 10^{-10}$  millibar, described in detail elsewhere.<sup>19</sup>

For electrical measurements, three separate samples were prepared; a native oxide starting surface, a  $(\text{NH}_4)_2\text{S}$  treated surface, and a Si IPL. Subsequently, 10 nm of  $\text{HfO}_2$  was deposited, followed by a post deposition anneal at 500 °C for 60 s in  $\text{N}_2$ . MOS capacitors (MOSCAPs) were formed with *ex-situ* e-beam Pd gate metal contacts deposited through a shadow mask with an area of  $8.65 \times 10^{-5} \text{ cm}^2$ . For back side Ohmic contacts, an e-beam evaporated Ni/Au/Ge

stack was used. Finally, a post metallization anneal (PMA) at 350 °C for 30 s in  $\text{N}_2$  was performed and C-V measurements taken after PMA.

XPS was utilized using a monochromated x-ray source ( $h\nu = 1486.7 \text{ eV}$ ) and a seven channel hemispherical analyzer operating at a pass energy of 20 eV. Core level spectra were taken of the As  $2p_{3/2}$ , As  $3d$ , In  $3d_{5/2}$ , In  $4d$ , Al  $2p$ , C  $1s$ , O  $1s$ , Hf  $4f$  (as well as S  $2p$  and Si  $2p$  for  $(\text{NH}_4)_2\text{S}$  and Si IPL samples, respectively).

## RESULTS

Figure 1 shows the As  $3d$  core level spectra for these four treated surfaces as well as for the native oxide prior to any treatment, without any annealing to highlight the effect of the chemical treatments. Typically, for surface chemistry studies involving arsenic containing compounds, the As  $2p$  core level is used to present detailed surface chemical analysis due to its significantly increased surface sensitivity relative to the As  $3d$  core level.<sup>20</sup> However, in this study, the intrinsically narrow peak width of the As  $3d$  core level (due to the smaller core-hole life time and correspondingly smaller Lorentzian component) is utilized. This allows for easier deconvolution of the peaks, especially considering the small binding energy (BE) separation between the individual peak components,<sup>21</sup> as will be discussed later. All peak deconvolutions and trends in the changes of the surface compositions from the As  $3d$  spectra were correlated to those from the corresponding higher BE peaks by concurrently fitting the As  $2p$  spectra, however, due to the increased error associated with the broader peaks, for clarity, only As  $3d$  spectra are presented here.

For the native oxide sample, evidence of the bulk As-InAl peak is detected at  $40.85 \pm 0.025 \text{ eV}$ , as well as As  $1+$ , As  $3+$  and As  $5+$  peaks (corresponding to  $\text{As}_2\text{O}_3$ ,

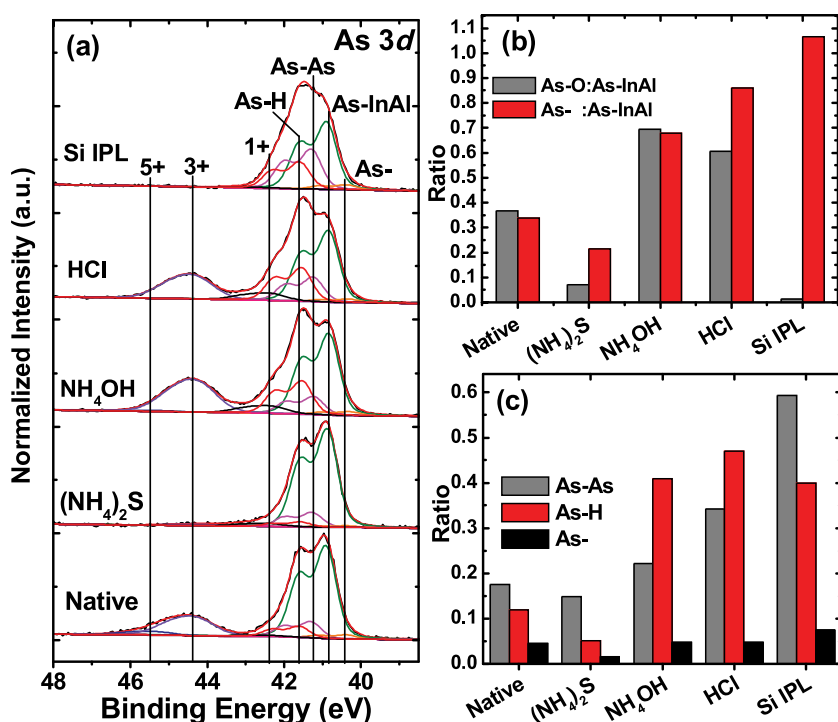


FIG. 1. (a) As  $3d$  core level spectra after various wet chemical treatments and amorphous silicon interfacial passivation layer deposition. (b) The ratio of As-O and As surface state peak areas to the As-InAl bulk peak from the fitted spectra and (c) the ratio of individual surface state peak areas to the bulk peak.

As<sub>2</sub>O<sub>3</sub>, and As<sub>2</sub>O<sub>5</sub>) with BE separations from the bulk peak of 1.50 eV, 3.35 eV, and 4.44 eV, respectively. There are 3 other peaks also detected, labeled as As-As, As-H, and As-, at 0.4 eV, 0.7 eV, and -0.44 eV from the bulk peak, respectively.<sup>8,22</sup> It is worth pointing out that the exact nature of these states is still a matter of investigation with a number of different studies claiming varying assignments.<sup>21–25</sup> For example, while our assignment of As-H in this case is consistent with the binding energy position reported by Beerbom *et al.* in Ref. 22, As-H itself would be unlikely to survive the elevated temperatures seen by the sample in the ALD reactor, and as such further work is needed to accurately identify the exact chemical composition of the peaks. However, it is clear that these are surface related features, energetically consistent with the breaking of substrate As bonds, likely forming As dimer, anti-site, hydride, or metallic like bonds. The concentration of these surface states is greater than that typically seen on the similar InGaAs surface,<sup>8</sup> particularly in relation to the presence of the As-H peak, suggesting that this surface is more chemically reactive than Ga containing compounds.

Comparing first the wet chemical treatments, one notes that the (NH<sub>4</sub>)<sub>2</sub>S is effective at removing the As-O states close to the XPS detection limits, with only a residual As 1+ state seen close to detection limits, which is likely due to the formation of As-S states.<sup>8,26,27</sup> The As-H state is also seen to decrease in concentration, with only a minor change in the concentration of As-As bonding detected. The NH<sub>4</sub>OH and HCl treated surfaces both show similar dramatic changes. While the concentration of As-O is seen to increase relative to the native oxide sample, this is likely due to re-oxidation of the surfaces during the 7 min after removal from solution and transfer to UHV for scanning, and may be indicative of increased surface roughness or reactivity of the surface after etching. The biggest change however is seen in the concentration of surface states detected, with a large increase (>1 monolayer) of As-As and As-H states observed.

On the Si IPL sample, As-O is below XPS detection limits however, the level of As surface states detected is the

greatest of all the surfaces studied. This indicates that while the Si is effective at scavenging oxygen from the less thermodynamically stable As oxides to form Si-O, this process results in the disruption of the semiconductor surface. In particular, the As-As state is greatly increased relative to the other samples, with As-H detected at a similar level to that of the NH<sub>4</sub>OH and HCl treated surfaces, as clearly indicated by the ratio of the substrate peak area to that from the individual peak components in Figure 1(c). It is possible that the As-As peak also contains a contribution from As-Si bonds, which would appear at a higher binding energy than the As-InAl peak based on the electronegativity of the elements.

HfO<sub>2</sub> was subsequently deposited by ALD (15 cycles) on three of these samples, (native, (NH<sub>4</sub>)<sub>2</sub>S, and Si IPL) to determine what interactions take place during the deposition process, and whether it would be possible to rely on the reported ALD “clean up” effect<sup>28</sup> to improve the interfacial characteristics by removing oxide and surface states. Figure 2(a) shows the As 3d core level spectra immediately after *in-situ* HfO<sub>2</sub> deposition, while 2(b) shows the corresponding change in total oxide and surface state peak areas to the bulk peak. For the native oxide and (NH<sub>4</sub>)<sub>2</sub>S treated surface, there is a decrease in the concentration of As-O upon ALD, likely due to the “clean up” effect, with As-O below detection limits on the (NH<sub>4</sub>)<sub>2</sub>S treated surface. On the native oxide and Si IPL samples, an increase in the surface state concentration after ALD is also observed, with no change seen on the (NH<sub>4</sub>)<sub>2</sub>S treated surface, suggesting that the sulfur is playing a role in enhancing the stability of the interface.

Considering next the In 3d<sub>5/2</sub> spectra for the same samples, before (with no prior sample heating) and after ALD in Figures 3 and 4, respectively, similar trends take place. For the native oxide sample, the In-AlAs bulk peak at 444.38 ± 0.025 eV is observed, as well as 3 oxide states, labeled In 1+, In 3+, and In-OH, separated from the bulk peak by 0.45 eV, 0.82 eV, and 1.25 eV, respectively, and tentatively assigned to In<sub>2</sub>O, In<sub>2</sub>O<sub>3</sub>, and an In hydroxide state (In(OH)<sub>3</sub>).<sup>21,29</sup> There is also some evidence for the presence of a lower binding energy peak, labeled In-, shifted from the

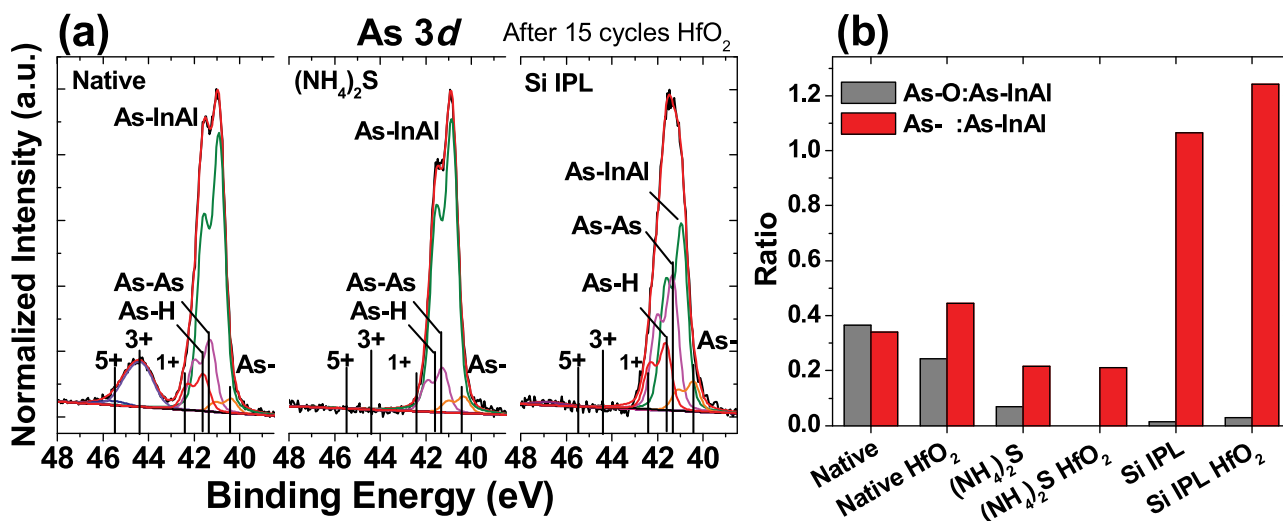


FIG. 2. (a) As 3d core level spectra after 15 cycles of HfO<sub>2</sub> deposition by ALD. (b) The peak area ratio of As-O and As surface states to the bulk peak area before and after deposition.



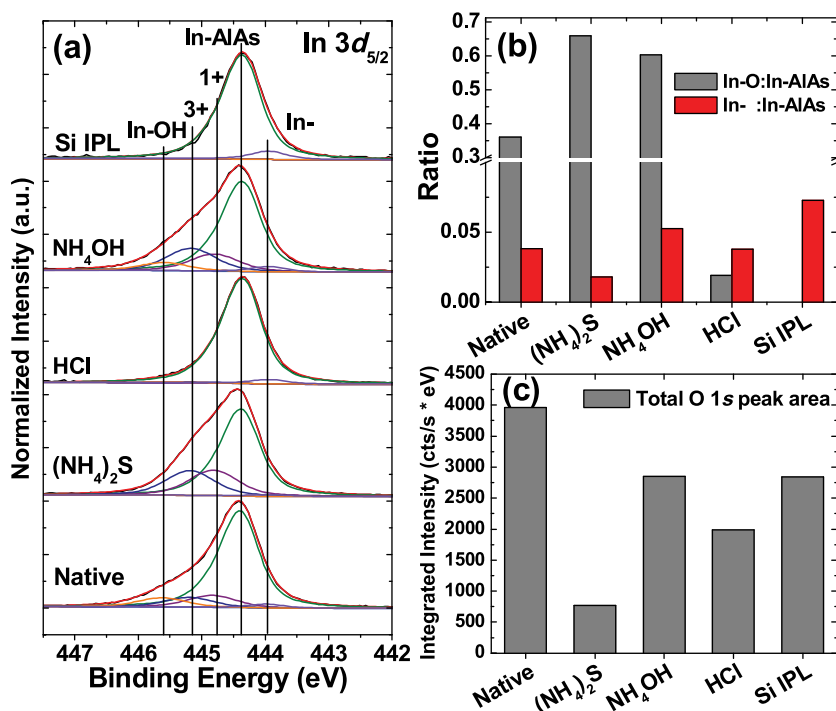


FIG. 3. (a) In 3d<sub>5/2</sub> core level spectra after various wet chemical treatments and amorphous silicon interfacial passivation layer deposition. (b) The ratio of In-O and In surface state peak areas to the In-AlAs bulk peak from the fitted spectra and (c) the total integrated peak area from the O 1s core level showing changes in surface oxygen concentration.

bulk peak by  $-0.40$  eV, however this is close to detection limits on this sample.

It is important to comment on the natural lineshape of the In-AlAs peak for this core level, as there is an inherent asymmetry observed which complicates the peak deconvolution.<sup>30</sup> This manifests itself as a broadening at the higher binding energy side of the peak. Various permutations of the peak fitting process have been undertaken to describe this lineshape, incorporating various lineshape functions. The traditional Doniach-Sunjić for metallic elements is not able to accurately describe the lineshape, and it has been found that incorporating an additional Lorentzian component at the higher binding energy side of the peak gives the most consistent deconvolution. This is most clearly evident in the HCl etched surface, which is the most effective chemical treatment at removing In-oxide states, here at the detection limits of the XPS. Based on the As 3d spectra and the increased concentration of As-O and As surface states, this suggests that the HCl etch leaves the surface predominantly As terminated.

The NH<sub>4</sub>OH treated surface shows a similar profile to the native oxide surface, although with an increased

concentration of oxide states detected. This could be an indication of roughening of the surface as a result of the etch and resulting in an increased surface area, or an increase in surface reactivity. Based on the total peak area of the O 1s core levels, plotted in Figure 3(c), there is an overall reduction in the concentration of O present on the surface after NH<sub>4</sub>OH treatment, indicating that the treatment is playing a role in removing native oxides. For the spectra from the (NH<sub>4</sub>)<sub>2</sub>S treated surface, two large In 1+ and 3+ peaks are detected, however, correlating this to the data from the O 1s peaks, which shows the lowest overall oxygen concentration on this sample, it is most likely that these are mostly due to the formation of In-S bonds at the surface. Comparing the intensity of these peaks to those observed on other In containing III-V materials, this concentration of In-S formation is quite significant, with a concentration greater than a monolayer, again reflecting the increased reactivity compared to InP and InGaAs.<sup>8</sup> From the S 2p spectra (not shown), the increased concentration of sulfur present relative to that seen on GaAs, InGaAs, and InP after (NH<sub>4</sub>)<sub>2</sub>S treatment is further confirmed by a greater integrated peak intensity. There is also no change detected in the concentration or chemical state of

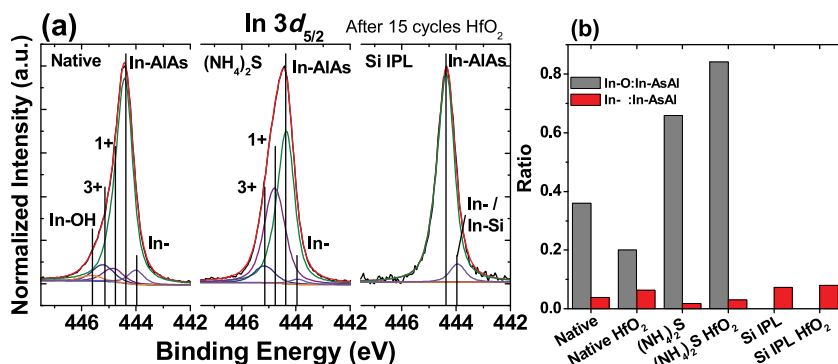


FIG. 4. (a) In 3d<sub>5/2</sub> core level spectra after 15 cycles of HfO<sub>2</sub> deposition by ALD. (b) The peak area ratio of In-O and In surface states to the bulk peak area before and after deposition.

the sulfur present on the surface throughout the experiment, remaining bonded to In (and possibly Al) after exposure to the ALD reactor at 250 °C and upon subsequent HfO<sub>2</sub> deposition.

Examination of the final sample after Si IPL formation indicated that there is no evidence of In-O within detection limits, similar to the results for the HCl etched surface. This indicates that the Si is effective at scavenging O from the In oxides to form SiO<sub>2</sub>. The reduction in O 1s peak area on this sample is most likely due to attenuation of the interfacial oxide due to the Si overlayer, with the O primarily located at the interface, and not due to removal of O from the system. The highest In-concentration is also seen on this sample, with a possible contribution from In-Si enhancing the contribution, and is a possible reflection on increased interfacial disorder being generated at this interface as a result of the deposition, consistent with the data from the As 3d core levels.

Upon HfO<sub>2</sub> deposition in Figure 4, a decrease in the concentration of In-O on the native oxide sample is detected as a result of interaction between the TDMA-Hf precursor and the oxide states. This is accompanied by a slight increase in In-bonds, suggesting the decomposition of indium oxides leaves broken In bonds at the surface. However, on the (NH<sub>4</sub>)<sub>2</sub>S treated surface, there is an overall increase in the combined In 1+ and In 3+ states, and primarily in the In 1+ form, most likely due to a transfer of sulfur, previously bonded to either As or Al, to form increased levels of In-S bonds.<sup>8</sup> On the Si IPL sample, there is no change in the In 3d spectra, with the passivation layer proving effective at preventing ALD precursor interaction with the substrate. This behavior is consistent with the enthalpy of formation for HfO<sub>2</sub> (−1144.7 kJ/mol) relative to that for SiO<sub>2</sub> (−910.7 kJ/mol) and In-oxides such as In<sub>2</sub>O<sub>3</sub> (−925.8 kJ/mol).<sup>31</sup>

The Al 2p core level spectra, shown in Figure 5(a), for the native oxide sample indicates the presence of the Al-InAs bulk peak at 73.64 eV, with 2 oxide states, attributed to Al<sub>2</sub>O<sub>3</sub> and an Al-OH state (possibly Al(OH)<sub>3</sub>), at 74.45 eV and 75.2 eV, respectively. (NH<sub>4</sub>)<sub>2</sub>S and NH<sub>4</sub>OH treatments are observed to produce almost identical results, with the concentration of Al-O states reduced by 60% on both surfaces, relative to the native oxide surface. Similar to the results seen in the In 3d spectra, the HCl treatment is the most effective at removing Al-O, particularly Al<sub>2</sub>O<sub>3</sub>, which is below XPS detection limits. On the Si IPL sample, the decrease in Al-O is much less dramatic, with only 18% reduction in the total Al-O concentration relative to the native oxide sample, with no preference for decrease shown between the Al<sub>2</sub>O<sub>3</sub> or Al-OH states (both are seen to decrease by the same percentage). This suggests there is limited interaction between the IPL and the aluminum oxides in terms of oxide transfer to form Si-O, with the more thermodynamically stable Al-O remaining at the interface.

The Si 2p core level spectra after IPL deposition is shown in Figure 5(c) and indicates that in addition to a peak related to the amorphous silicon at 100.0 eV, there is a large Si-O peak (102.3 eV) corresponding to the formation of a silicate. There is also an intermediate peak detected at 101.0 eV. From angular resolved XPS measurements (not shown), it appears that this intermediate state is located at the surface of the Si IPL (integrated peak area decreases with more bulk sensitive measurements while oxide and Si-Si peak areas remain essentially unchanged). This is possibly related to the formation of As-Si bonds<sup>32</sup> which diffuse to the surface of the Si IPL, and would explain the increased As surface state peak area seen in the As 3d core level spectra. After HfO<sub>2</sub> deposition, the integrated peak area of this peak decreases, possibly through oxidation of these states to form

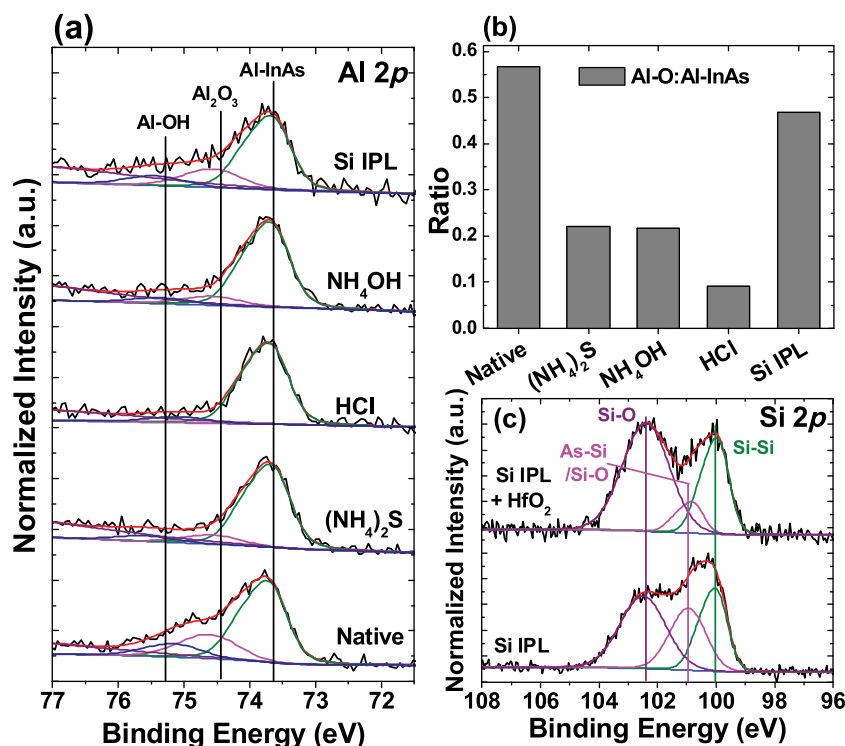


FIG. 5. (a) Al 2p core level spectra after various wet chemical treatments and amorphous silicon interfacial passivation layer deposition. (b) The ratio of Al-O peak areas to the Al-InAs bulk peak from the fitted spectra and (c) the fitted Si 2p core level spectra before and after HfO<sub>2</sub> deposition from the Si IPL sample.

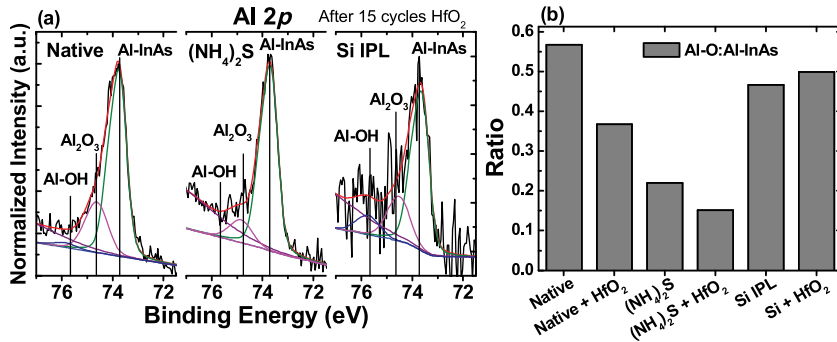


FIG. 6. (a) Al 2p core level spectra after 15 cycles of HfO<sub>2</sub> deposition by ALD. (b) The peak area ratio of Al-O to the bulk peak area before and after deposition.

increased concentrations of silicate, again consistent with the increase in peak area of the oxide peak at 102.3 eV in the Si 2p spectra. This oxidation may then also explain the increase in As surface states on the Si IPL sample after HfO<sub>2</sub> deposition, with the residual elemental As species remaining at the interface after Si oxidation during ALD. It should be noted that a silicon sub-oxide origin for this intermediate peak, or a combination of both As-Si bonding and sub-oxide states cannot be fully ruled out, as these would be expected to have a similar binding energy. Given the temperatures employed here, Si-O formation seems most plausible.

The Al 2p spectra from the native, (NH<sub>4</sub>)<sub>2</sub>S, and Si IPL samples after HfO<sub>2</sub> deposition are shown in Figure 6. For the native oxide sample, a decrease in the concentration of the Al-O at the interface upon ALD is again observed, as well as a decrease in the concentration of Al-OH states, consistent with metal precursor interactions with -OH bonds during typical ALD reactions. On the (NH<sub>4</sub>)<sub>2</sub>S sample, a decrease in the concentration of the Al-O peaks present on the surface is also detected; however, this could also be evidence of Al-S bonds being converted to In-S. It should be noted that on the Si IPL sample, due to the low photoionization cross section of the Al 2p core level and attenuation of the substrate by both HfO<sub>2</sub> and the Si IPL, there is a very low signal to noise ratio and as such, although the oxide to bulk ratios are not observed to change after ALD, as expected, there is a large error associated with this measurement.

Comparing the Hf 4f core level spectra in Figure 7(a), as well as the fitted peak areas in Figure 7(b), there is a virtually identical peak area and binding energy position for the Hf 4f peak on the native oxide and (NH<sub>4</sub>)<sub>2</sub>S treated surfaces. This indicates that both surfaces experience the same ALD growth rate and that the HfO<sub>2</sub> is in the same chemical state on both surfaces. However, on the Si IPL sample, there is a clear increase in the concentration of Hf-O states present on the Si IPL surface, based on the peak areas. There is also an increase in the peak binding energy position by 0.4 eV, suggesting a change in the chemical composition. This is consistent with the changes seen in the Si 2p spectra after ALD, indicating that there is significant interaction taking place between the deposited HfO<sub>2</sub> and the Si IPL, and that at least part of the deposited layer is in the form of Hf-silicate.

Figure 8 shows room temperature, multi-frequency C-V characteristics for InAlAs/HfO<sub>2</sub> MOS capacitors with different surface preparations; (a) native oxide, (b) (NH<sub>4</sub>)<sub>2</sub>S, and (c) Si IPL (1 nm Si + 10 nm HfO<sub>2</sub> = 11 nm total overlayer for this sample). All samples show very large frequency

dispersion in the maximum capacitance corresponding to an *ac* defect response dominated by defects at the HfO<sub>2</sub>/InAlAs interface and the possible contribution of defects located within the HfO<sub>2</sub> very near the HfO<sub>2</sub>/InAlAs interface.<sup>32</sup> Samples with the Si IPL and a native oxide show an additional trap response at 100 Hz in the depletion region. These C-V characteristics suggest that although the native oxide and Si IPL samples showed variations in the interfacial

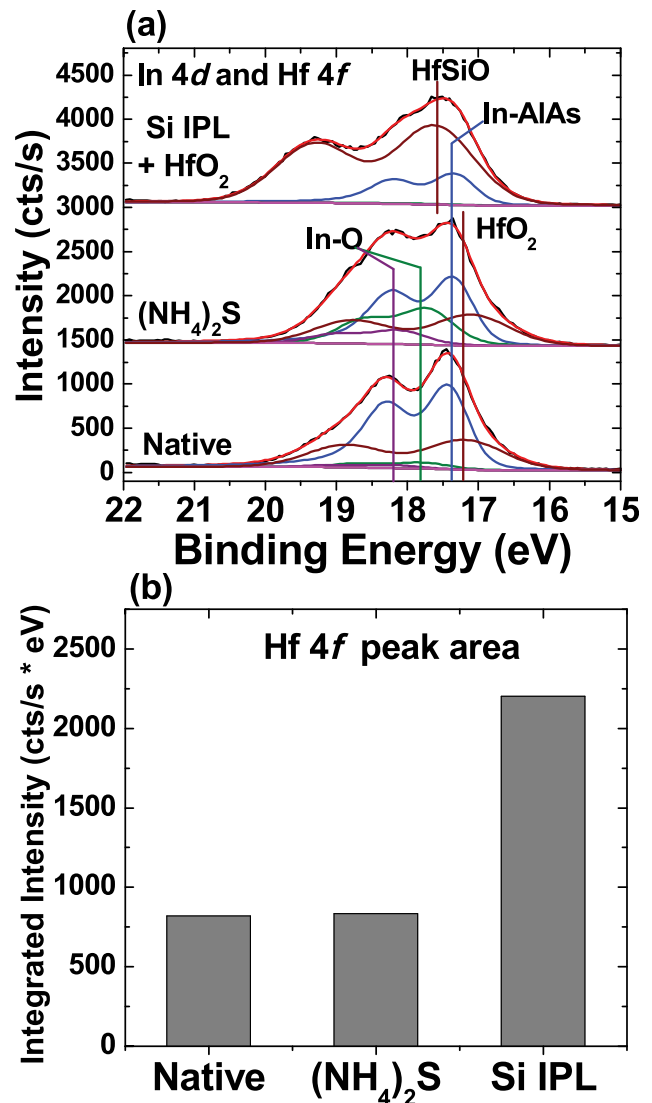


FIG. 7. (a) In 4d and Hf 4f core level spectra after 15 cycles of HfO<sub>2</sub> deposition by ALD. (b) Integrated peak area of Hf 4f core level spectra indicating increase in Hf-O related species on Si IPL sample.



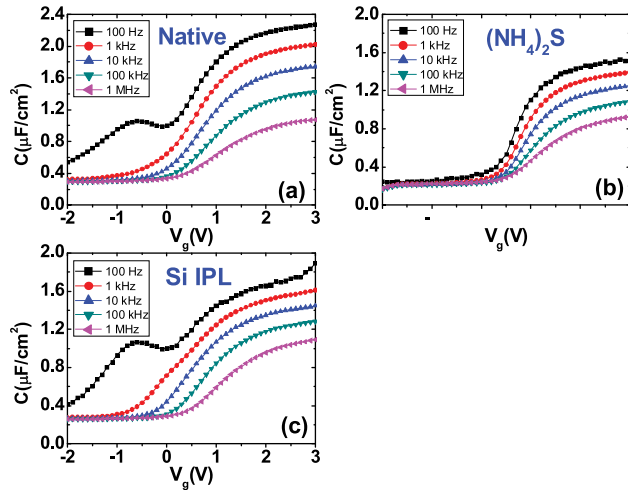


FIG. 8. Room temperature multi-frequency C-V characteristics for InAlAs/HfO<sub>2</sub> MOS capacitors with (a) native oxide, (b) (NH<sub>4</sub>)<sub>2</sub>S passivation and (c) Si IPL. All of the samples show large frequency dispersion in the maximum capacitance. Additional trap response in the depletion region is observed for Si IPL and native oxide samples at 100 Hz.

chemistry in the XPS measurements, the observed depletion trap response in C-V could be due to a similar chemical state present at these interfaces. The trap response in the depletion region can possibly be attributed to the high concentration of As surface states detected on this sample from XPS. The frequency response in these devices is similar to that seen in GaAs MOSCAPs, i.e., a large amount of frequency dispersion and a relative lack of free carriers<sup>33</sup> (see the 77 K measurements in Fig. 9). It is now generally accepted that this frequency dispersion cannot be modeled in the traditional manner employed for Si-based devices. To accurately model this response requires a revised interface trap capacitance calculation that incorporates tunneling of carriers into defect states that reside away from the crystalline semiconductor interface. Two models that include this tunneling mechanism are the disorder induced gap states (DIGS) model<sup>34,35</sup> and border traps.<sup>36,37</sup> Our current understanding of the origin of this frequency response necessitates that the defect states are associated with the disruption of the III-V interface and not with border traps located throughout the bulk of the high-k dielectric. These states include dangling bonds and As-As distributed within the first 5–10 Å from the interface. It is noted that, regardless of whether the origin of the defects is due to border traps in the high-k dielectric or III-V interface disorder-related traps, such traps are located away from the

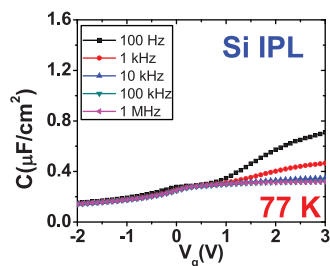


FIG. 9. Low temperature (77 K) C-V characteristics for InAlAs/HfO<sub>2</sub> MOS capacitors with a Si IPL. Very small change in measured capacitance as a function of gate voltage is observed, indicating a pinned Fermi level.

interface (but within 1 nm) and both models generally produce the observed frequency dispersion behavior.

In order to determine to what extent  $D_{it}$  was playing a role in the C-V response at room temperature, measurements were also performed at 77 K. Figure 9 shows multi-frequency C-V characteristics for the Si IPL sample at 77 K. Only very small changes in the measured capacitance over the entire gate voltage range are observed, with similar results obtained for the other two samples. The trap time constant at 77 K is very large and traps generally do not have time to respond to the AC modulation signal.<sup>38,39</sup> As such, only the semiconductor response is typically detected. However, in this case, some trap response is still detected suggesting a very high  $D_{it}$  concentration. Low temperature measurements indicate that the surface Fermi level is severely pinned and only a very small modulation of the semiconductor surface potential as a function of gate voltage is observed. As a result of this pinning, the devices do not go into accumulation and the room temperature C-V characteristics are completely dominated by interface trap response, with only a small number of free carriers present. Since the surface Fermi level is severely pinned, the  $D_{it}$  as a function of bandgap energy cannot be accurately calculated as parameters required for the  $D_{it}$  calculation like the oxide capacitance and flat-band voltage cannot be extracted from the experimental C-V characteristics. Furthermore, as the surface potential does not change with gate voltage, the  $D_{it}$  as a function of bandgap energy cannot be determined, however an estimate of the  $D_{it}$  value needed to pin the Fermi level to this extent would put it at the high  $10^{13} \text{ cm}^{-2} \text{ eV}^{-1}$  level.

## CONCLUSIONS

Assessing the various surface treatments taking into account data from the As, In, and Al core levels, it is possible that a combination of etching in HCl to remove interfacial In and Al oxides, followed by an (NH<sub>4</sub>)<sub>2</sub>S treatment to remove As oxide and potentially decrease the concentration of As surface states, may provide a route to developing optimized initial processing conditions for samples prior to ALD and warrants further investigation. However, based on the results presented here, it is very likely that the concentration of surface related defect states will remain very high, which would have major implications for device performance. Despite (NH<sub>4</sub>)<sub>2</sub>S treatment showing the lowest concentration of interfacial oxides present on the InAlAs surface based on the chemical treatments investigated here, C-V measurements were still dominated by a  $D_{it}$  response, and the introduction of a Si IPL to help remove these states and mitigate oxidation prior to ALD, showed no improvement contrary to results observed for GaAs, with additional trap response seen in depletion possibly attributed to an increase in As surface states.

## ACKNOWLEDGMENTS

This work was supported by the Semiconductor Research Corporation FCRP Materials Structures and Devices Center and the National Science Foundation under

ECCS Award No. 0925844 for the U.S.-Ireland research collaboration. The authors from the Tyndall Institute acknowledge the financial support of Science Foundation Ireland (Grant No. 08/US/I1546).

- <sup>1</sup>J. del Alamo, *Nature (London)* **479**, 317 (2011).
- <sup>2</sup>J. Q. Lin, S. J. Lee, H. J. Oh, G. Q. Lo, D. L. Kwong, and D. Z. Chi, *IEEE Electron Device Lett.* **29**, 977 (2008).
- <sup>3</sup>C. L. Hinkle, M. Milojevic, A. M. Sonnet, H. C. Kim, J. Kim, E. M. Vogel, and R. M. Wallace, *ECS Trans.* **19**, 387 (2009).
- <sup>4</sup>S. Adachi and D. Kikuchi, *J. Electrochem. Soc.* **147**, 4618 (2000).
- <sup>5</sup>Y. Sun, Z. Liu, F. Machuca, P. Pianetta, and W. E. Spicer, *J. Vac. Sci. Technol. A* **21**, 219 (2003).
- <sup>6</sup>W. Melitz, J. Shen, T. Kent, A. C. Kummel, and R. Droopad, *J. Appl. Phys.* **110**, 013713 (2011).
- <sup>7</sup>F. S. Aguirre-Tostado, M. Milojevic, C. L. Hinkle, E. M. Vogel, R. M. Wallace, S. McDonnell, and G. J. Hughes, *Appl. Phys. Lett.* **92**, 171906 (2008).
- <sup>8</sup>B. Brennan, M. Milojevic, C. L. Hinkle, F. S. Aguirre-Tostado, G. Hughes, and R. M. Wallace, *Appl. Surf. Sci.* **257**, 4082 (2011).
- <sup>9</sup>J. J. Gu, A. T. Neal, and P. D. Ye, *Appl. Phys. Lett.* **99**, 152113 (2011).
- <sup>10</sup>V. Chobpattana, J. Son, J. J. M. Law, R. Engel-Herbert, C.-Y. Huang, and S. Stemmer, *Appl. Phys. Lett.* **102**, 022907 (2013).
- <sup>11</sup>T. Hoshii, S. Lee, R. Suzuki, N. Taoka, M. Yokoyama, H. Yamada, M. Hata, T. Yasuda, M. Takenaka, and S. Takagi, *J. Appl. Phys.* **112**, 073702 (2012).
- <sup>12</sup>M. Radosavljevic, B. Chu-Kung, S. Corcoran, M. K. Hudait, G. Dewey, J. M. Fastenau, J. Kavalieros, W. K. Liu, D. Lubyshev, M. Metz, K. Millard, W. Rachmady, U. Shah, and R. Chau, in *IEEE Conference Proceedings of International Electron Devices Meeting (IEDM)* (IEEE, New York, 2009), p. 319.
- <sup>13</sup>F. Xue, H. Zhao, Y.-T. Chen, Y. Wang, F. Zhou, and J. C. Lee, *Appl. Phys. Lett.* **98**, 082106 (2011).
- <sup>14</sup>H. Zhao, Y.-T. Chen, J. H. Yum, Y. Wang, F. Zhou, F. Xue, and J. C. Lee, *Appl. Phys. Lett.* **96**, 102101 (2010).
- <sup>15</sup>F. Xue, H. Zhao, Y.-T. Chen, Y. Wang, F. Zhou, and J. C. L. Lee, *Appl. Phys. Lett.* **99**, 033507 (2011).
- <sup>16</sup>A. Šilenas, Yu. Požela, K. Požela, V. Jucienė, I. S. Vasil'evskii, G. B. Galiev, S. S. Pushkarev, and E. A. Klimov, *Semiconductors* **47**, 372 (2013).
- <sup>17</sup>B. Benbakhti, J. S. Ayubi-Moak, K. Kalna, D. Lin, G. Hellings, G. Brammertz, K. De Meyer, I. Thayne, and A. Asenov, *Microelectron. Reliab.* **50**, 360 (2010).
- <sup>18</sup>V. Dimastrodonato, L. O. Mereni, R. J. Young and E. Pelucchi, *J. Cryst. Growth* **312**, 3057 (2010).
- <sup>19</sup>R. M. Wallace, *ECS Trans.* **16**, 255 (2008).
- <sup>20</sup>C. L. Hinkle, M. Milojevic, E. M. Vogel, and R. M. Wallace, *Appl. Phys. Lett.* **95**, 151905 (2009).
- <sup>21</sup>B. Brennan and G. Hughes, *J. Appl. Phys.* **108**, 053516 (2010).
- <sup>22</sup>M. Beerbom, T. Mayer, W. Jaegermann, D. R. Batchelor, and D. Schmeisser, *Anal. Bioanal. Chem.* **374**, 650 (2002).
- <sup>23</sup>M. V. Lebedev, D. Ensling, R. Hunger, T. Mayer, and W. Jaegermann, *Appl. Surf. Sci.* **229**, 226 (2004).
- <sup>24</sup>Z. Liu, Y. Sun, F. Machuca, P. Pianetta, and W. E. Spicer, *J. Vac. Sci. Technol. A* **21**, 212 (2003).
- <sup>25</sup>D. Paget, J. E. Bonnet, V. L. Berkovits, P. Chiaradia, and J. Avila, *Phys. Rev. B* **53**, 4604 (1996).
- <sup>26</sup>E. O'Connor, B. Brennan, V. Djara, K. Cherkaoui, S. Monaghan, S. B. Newcomb, R. Contreras, M. Milojevic, G. Hughes, M. E. Pemble, R. M. Wallace and P. K. Hurley, *J. Appl. Phys.* **109**, 024101 (2011).
- <sup>27</sup>L. Chauhan and G. Hughes, *Phys. Status Solidi A* **210**, 519 (2013).
- <sup>28</sup>M. Milojevic, C. L. Hinkle, F. S. Aguirre-Tostado, H. C. Kim, E. M. Vogel, J. Kim, and R. M. Wallace, *Appl. Phys. Lett.* **93**, 252905 (2008).
- <sup>29</sup>G. Hollinger, E. Bergignat, J. Joseph, and Y. Robach, *J. Vac. Sci. Technol. A* **3**, 2082 (1985).
- <sup>30</sup>B. Brennan, M. Milojevic, R. Contreras-Guerrero, H. C. Kim, M. Lopez-Lopez, J. Kim, and R. M. Wallace, *J. Vac. Sci. Technol. B* **30**, 04E104 (2012).
- <sup>31</sup>*CRC Handbook of Chemistry and Physics*, 92nd ed., edited by W. M. Haynes and D. R. Lide (CRC Press, 2011) 5-14-17.
- <sup>32</sup>D. A. Schmidt, T. Ohta, C.-Y. Lu, A. A. Bostwick, Q. Yu, E. Rotenberg, F. S. Ohuchi, and M. A. Olmstead, *Appl. Phys. Lett.* **88**, 181903 (2006).
- <sup>33</sup>G. Brammertz, A. Alian, D. H.-C. Lin, M. Meuris, M. Caymax, and W.-E. Wang, *IEEE Trans. Electron Devices* **58**, 3890 (2011).
- <sup>34</sup>A. M. Sonnet, C. L. Hinkle, D. Heh, G. Bersuker, and E. M. Vogel, *IEEE Trans. Electron Devices* **57**, 2599 (2010).
- <sup>35</sup>H. Hasegawa and T. Sawada, *Surf. Sci.* **98**, 597 (1980).
- <sup>36</sup>Y. Yuan, B. Yu, J. Ahn, P. C. McIntyre, P. M. Asbeck, M. J. W. Rodwell, and Y. Taur, *IEEE Trans. Electron Devices* **59**, 2100 (2012).
- <sup>37</sup>E. J. Kim, L. Q. Wang, P. M. Asbeck, K. C. Saraswat, and P. C. McIntyre, *Appl. Phys. Lett.* **96**, 012906 (2010).
- <sup>38</sup>S. M. Sze and K. K. Ng, *Physics of Semiconductor Devices*, 3rd ed. (Wiley-Interscience, New York, 2007), p. 221.
- <sup>39</sup>E. O'Connor, S. Monaghan, R. D. Long, A. O'Mahony, I. M. Povey, K. Cherkaoui, M. E. Pemble, G. Brammertz, M. Heyns, S. B. Newcomb, V. V. Afanas'ev, and P. K. Hurley, *Appl. Phys. Lett.* **94**, 102902 (2009).